Quasiclassical Trajectory Study of the Collision-Induced Dissociation Dynamics of Ar + CH_3SH^+ Using an Ab Initio Interpolated Potential Energy Surface†

Emilio Martínez-Núñez,*,‡ Saulo A. Vázquez,‡ F. Javier Aoiz,§ and Jesús F. Castillo§

Departamento de Química Física, Universidad de Santiago de Compostela, 15782 Santiago de Compostela, Spain, and Departamento de Química Física I, Facultad de Química, Universidad Complutense de Madrid, Spain

Received: May 4, 2005; In Final Form: July 12, 2005

Classical trajectory calculations have been performed to investigate the collision-induced dissociation (CID) of the CH_3SH^+ cation with Ar atoms. A new intramolecular potential energy surface for the CH_3SH^+ cation is evaluated by interpolation of 3000 ab initio data points calculated at the MP2/6-311G(d,p) level of theory. The new potential energy surface includes seven accessible dissociation channels of the cation. The present QCT calculations show that migration of hydrogen atoms, leading to the rearrangement $CH_3SH^+ \leftrightarrow CH_2SH_2^+$, is significant at the collision energies considered (6.5−34.7 eV) and that the formation of CH_3^+, CH_3S^+, and CH_2^+ cations takes place primarily by a "shattering" mechanism in which the products are formed just after the collision. The theoretical product abundances are found to be in qualitative agreement with the experimental data. However, at high collision energies, the calculated total cross sections for the formation of CH_3^+ and CH_2SH^+ cations are noticeably larger than the experimental determinations. Several features of the dynamics of the CID processes are discussed.

Introduction

The unimolecular dissociation of CH_3SH^+ species has been investigated experimentally by collisional activation,[1−3] mass spectrometry,[4−6] charge exchange,[7] and photoelectron photoion coincidence (PEPICO)[8] and theoretically by classical trajectory calculations.[9−11] Both theory and experiment show that the product branching ratios depend strongly on the mechanism of excitation of the CH_3SH^+ cation. In particular, mass spectrometry, charge exchange, and PEPICO techniques give rise to product branching ratios in good agreement with RRKM[6] and classical trajectory calculations[9,10] that use microcanonical sampling. Experiments and theory agree that CH_2SH^+ is the most probable product of dissociation. By contrast, when CH_3SH^+ is excited by collisions with Ar, the main product channel is $CH_3^+ + SH$, which is far from being the lowest energy dissociation channel, as can be seen in Figure 1. Both experiment[1−3] and theory[11] show that the CH_3^+ product is 3−4 times more abundant than the CH_2SH^+ product. This observation indicated that the CID process is nonstatistical. Ng and co-workers[1−3] concluded that the translational to vibrational (T → V) energy transfer efficiency is higher for the low-frequency vibrational modes of CH_3SH^+ (particularly, the CS stretch) and that the couplings between these modes and the high-frequency vibrational modes are weak.

Very recently, these conclusions were corroborated by quasiclassical trajectory (QCT) calculations.[11] However, although these QCT results were in reasonably good agreement with the experimental data with regard to the relative abundances of the major product ions, the QCT cross sections predicted at the highest energies investigated were about 4 times higher than the experimental results.[11] It was suggested that the incompleteness of the potential energy surface (PES) used in the calculations (i.e., we only considered channels labeled I−III in Figure 1) could be an important source of discrepancies.[11] For this reason, in the present work we have undertaken a QCT study of the collision-induced dissociation of CH_3SH^+ at collision energies between 6.5 and 34.7 eV using a new intramolecular PES that includes four additional channels (IV to VII in Figure 1). The new intramolecular potential was constructed by interpolation of 3000 ab initio data points at the MP2/6-311G(d,p) level of theory using the Gaussian 98 suite of programs.[12] In addition to the calculation of product branching ratios, new features on the dynamics of $Ar + CH_3SH^+$, not investigated in the previous study,[11] will be discussed in the present work.

Computational Details

A. Potential Energy Surface. The PES employed in the QCT calculations consists of an intramolecular potential energy function for CH_3SH^+, V_{CH3SH^+}, and an intermolecular potential that takes the Ar-CH_3SH^+ van der Waals interactions into account, constructed as a sum of pair-potentials V_{Ar-Xi}

$$V_{ArCH_3SH^+} = V_{CH_3SH^+} + \sum_{i=1}^{6} V_{Ar-X_i} \qquad (1)$$

The intermolecular part of the potential $\sum_{i=1}^{6} V_{Ar-X_i}$ is the same as that used in our previous QCT study,[11] and the reader is referred to that reference for a thorough description. We only recall here that the intermolecular potential function was fitted to more than 80 single-point QCISD(T)/6-311G(d,p) calculations at various relevant Ar-CH_3SH^+ relative geometries using the geometry calculated by a QCISD/6-311G(d,p) optimization for the CH_3SH^+ radical.

† Part of the special issue "William Hase Festschrift".

* Corresponding author. E-mail: qfemilio@usc.es.
‡ Universidad de Santiago de Compostela.
§ Universidad Complutense de Madrid.

10.1021/jp052325d CCC: $33.50
Published on Web 10/18/2005

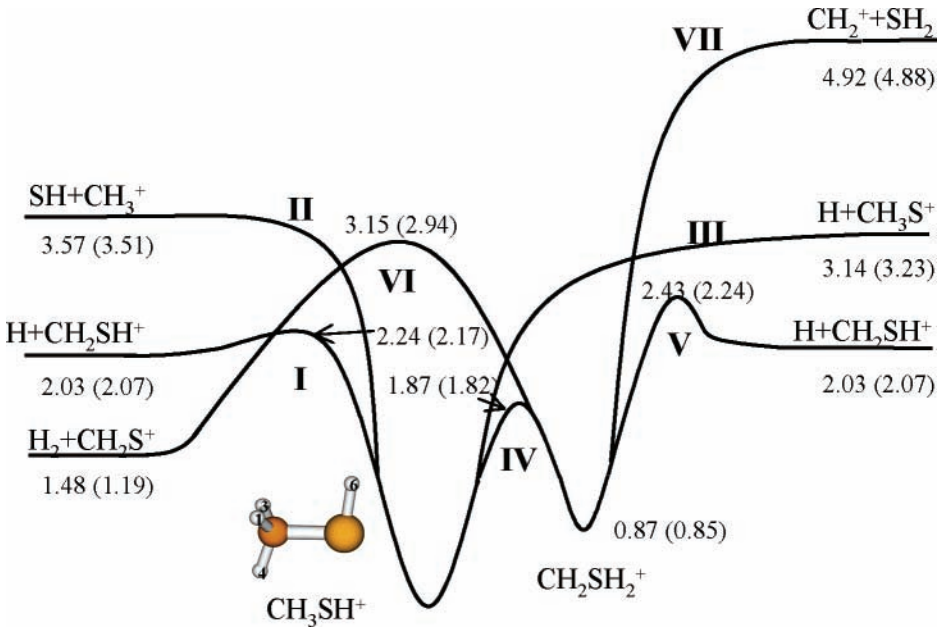

Figure 1. Potential energy profile (not to scale) for the rearrangement and fragmentation reactions of CH_3SH^+ studied in this work. The reaction barriers and endothermicities (including zero-point energy corrections), obtained by MP2/6-311G(d,p) and QCISD(T)/6-311G(d,p)/QCISD/6-311G-(d,p) (in parentheses), are given in eV.

As pointed out in the Introduction, the analytical intramolecular potential used in our previous QCT calculations involved only the following dissociation channels (see also Figure 1)

$$CH_3SH^+ \rightarrow CH_2SH^+ + H \qquad \text{(I)}$$

$$CH_3SH^+ \rightarrow CH_3^+ + SH \qquad \text{(II)}$$

$$CH_3SH^+ \rightarrow CH_3S^+ + H \qquad \text{(III)}$$

To determine the extent to which the differences between our previous QCT calculations and experiment are caused by the lack of additional accessible dissociation channels, which may have an important contribution to the total cross section at high collision energies, in the present study we have constructed a new analytical intramolecular potential that includes additional channels. This PES has been obtained by interpolation of 3000 energies, gradients, and Hessians at the MP2/6-311G(d,p) level of theory, following the technique of Collins and co-workers as implemented in the GROW package.[13−15] This level of theory has been selected by its good performance in comparison with higher level QCISD(T)/6-311G(d,p) calculations.[16] It should be mentioned that for some configurations the MP2 wave function contains a significant spin contamination, which may cause inaccuracies in the PES. Nonetheless, we expect the MP2/6-311G(d,p) level to be valid for the purposes of describing CID of CH_3SH^+ with Ar, at least qualitatively or semiquantitatively, because in general the PES is represented reasonably well at this level of theory. It is also important to indicate that there was a mistake in the interpretation of our previous ab initio calculations of ref 16: the transition state that was believed to link CH_3SH^+ with products $CH_2S^+ + H_2$ (named TS2 in that reference) is in fact a transition state for the $H + CH_2SH^+ \rightarrow CH_2S^+ + H_2$ bimolecular reaction. Actually, in this study we were not able to find any transition state connecting CH_3SH^+ with the $CH_2S^+ + H_2$ products. However, we optimized a transition state connecting $CH_2SH_2^+$ with $CH_2S^+ + H_2$ (with a relative energy of 3.15 eV, as seen in Figure 1). This new transition state is depicted in Figure 2, along with its main geometrical parameters.

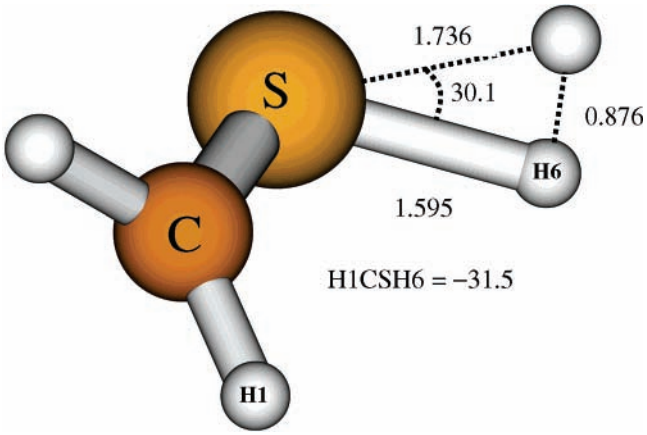

Figure 2. Transition state connecting $CH_2SH_2^+$ with $CH_2S^+ + H_2$, optimized at the MP2/6-311G(d,p) level. Bond distances in Å and angles in degrees.

Apart from the above-mentioned three channels, in the present dynamical study we also consider the following channels (see Figure 1):

$$CH_3SH^+ \rightarrow CH_2SH_2^+ \qquad \text{(IV)}$$

$$CH_2SH_2^+ \rightarrow CH_2SH^+ + H \qquad \text{(V)}$$

$$CH_2SH_2^+ \rightarrow CH_2S^+ + H_2 \qquad \text{(VI)}$$

$$CH_2SH_2^+ \rightarrow CH_2^+ + SH_2 \qquad \text{(VII)}$$

Therefore, in the new PES there are two additional dissociation channels, which give rise to CH_2^+ and CH_2S^+, and CH_2SH^+ may be formed from either CH_3SH^+ or from the $CH_2SH_2^+$ isomer (both being linked by channel IV).

For the construction of the PES, we first selected a total of 600 points (at the MP2/6-311G(d,p) level) from the reaction minimum energy paths (MEP) of the seven channels and used these data points as an initial guess for developing the PES. Subsequently, the number of data points and, concomitantly,

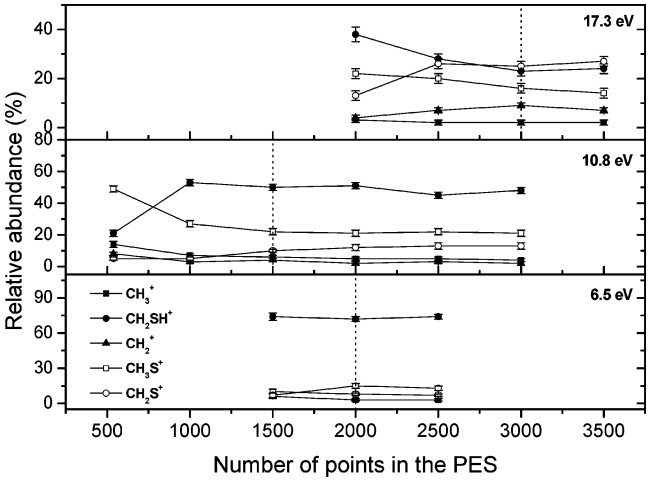

Figure 3. Convergence on the branching ratios as a function of the number of points in the interpolated PES for three different vibrational energies of CH_3SH^+.

the accuracy of the PES were enhanced gradually by using an iterative process in which classical trajectories are propagated to explore the relevant regions of the configuration space of the system.[13−15] For each trajectory, one or more of the configuration points defining the trajectory is selected as a new data point. These classical trajectories were initialized by the efficient microcanonical sampling (EMS) procedure[17,18] at three CH_3SH^+ vibrational energies (specifically, 6.5, 10.8, and 17.3 eV), chosen to essentially cover the whole range of vibrational energies of excited CH_3SH^+ molecules by collision with Ar. At each of these vibrational energies, the convergence on the CH_3^+, CH_2SH^+, CH_2^+, CH_3^+, and CH_2S^+ product abundances was checked by running batches of 2000 trajectories using in this case a normal mode sampling[19,20] to select the CH_3SH^+ + Ar initial conditions. Convergence in the product yields was achieved from 1500, 2000, and 3000 data points in the PES for the vibrational energies of 10.8, 6.5, and 17.3 eV, respectively (see Figure 3).

B. QCT Details. The initial conditions for the QCT calculations were selected to mimic the experimental conditions of the CID studies of Ng and co-workers.[1,2] Specifically, the CH_3SH^+ cation was considered to be in the ground vibronic state and with a rotational temperature of 150 K. The initial distance between Ar and the center-of-mass of CH_3SH^+ was 19 Å, and the impact parameter, b, was chosen randomly between 0 and b_{max} using the relation $b = (R_i)^{1/2}b_{max}$, where R_i is a freshly generated random number between 0 and 1 and b_{max} ranges from 2.5 to 3.3 Å. To run the trajectories, we have used our own trajectory code interfaced with the subroutines of Grow that calculate the energy and potential derivatives of the PES. We have run batches of 5000 trajectories at the following collision energies: 6.5, 8.7, 10.8, 13.0, 15.2, 17.4, 19.5, 21.7, 23.8, 26.0, 28.2, 30.4, 32.5, and 34.7 eV. The equations of motion were integrated by using a combined fourth-order Runge−Kutta and six-order Adams−Moulton predictor-corrector algorithm with a fixed time step of 0.01 fs, which guaranteed conservation of the total energy to better than one part in 10^4. A total of 32 reaction channels are possible when the possibility of hydrogen migration (via channel IV) is taken into account. Trajectories were halted when one of the following criteria was met: (a) All interatomic distances between two molecular fragments of CH_3SH^+ were greater than 6 Å. (b) The vibrational energy over the zero-point energy (ZPE) of the scattered CH_3SH^+ ion was lower than 2.24 eV, which is the barrier height (including ZPE corrections) for the lowest-energy dissociation process, that is, $CH_3SH^+ \rightarrow CH_2SH^+ + H$; in that case the trajectory was counted as nonreactive. (c) The vibrational energy of the scattered CH_3SH^+ ion was higher than 2.24 eV but lower than 3.14 eV (that is, below the dissociation energy D_0 for the $CH_3S^+ + H$ channel; see Figure 1); in this case the trajectory was considered to lead to $CH_2SH^+ + H$. (d) The total elapsed time reached 5 ps; in such a case the trajectory was randomly assigned to channel I, II, or III (we neglected here the possibility of fragmentation via other reactive channels) by using the RRK branching ratios of ref 9 as statistical weights, as explained in our previous QCT study.[11] This statistical assignment of reactive events is a reasonable approximation because the vibrational energy redistribution is accomplished after 5 ps. Besides, the percentage of trajectories we had to assign by this statistical calculation was 7% of the total number of reactive events at most.

TABLE 1: Percentages for Each of the Product Ions, Calculated with Respect to the Total Number of Trajectories Halted by Criterion a

collision energy (eV)	CH_3^+	CH_2SH^+	CH_2S^+	CH_2^+	CH_3S^+
6.5	100 ± 7.6	0	0	0	0
8.7	93.7 ± 5.0	4.2 ± 0.4	0.3 ± 0.3	1.1 ± 0.6	0.7 ± 0.4
10.8	91.6 ± 3.9	5.6 ± 0.4	0.8 ± 0.3	1.3 ± 0.5	0.7 ± 0.4
13.0	87.9 ± 3.1	7.6 ± 0.4	1.0 ± 0.3	2.5 ± 0.6	1.0 ± 0.4
15.2	87.2 ± 2.8	8.1 ± 0.4	1.0 ± 0.3	2.6 ± 0.5	1.1 ± 0.4
17.4	85.6 ± 2.5	7.2 ± 0.4	1.3 ± 0.3	3.5 ± 0.6	2.4 ± 0.5
19.5	82.4 ± 2.4	7.9 ± 0.4	2.2 ± 0.4	5.2 ± 0.7	2.3 ± 0.4
21.7	79.5 ± 2.2	8.8 ± 0.4	2.0 ± 0.4	6.4 ± 0.7	3.3 ± 0.5
23.9	78.1 ± 2.2	10.6 ± 0.5	2.8 ± 0.4	5.7 ± 0.7	2.8 ± 0.5
26.0	77.4 ± 2.2	9.3 ± 0.4	2.2 ± 0.3	6.9 ± 0.7	4.2 ± 0.6
28.2	73.0 ± 2.0	10.5 ± 0.5	2.3 ± 0.3	9.3 ± 0.8	4.9 ± 0.6
30.4	72.0 ± 1.9	10.3 ± 0.5	2.0 ± 0.3	10.1 ± 0.8	5.6 ± 0.6
32.5	71.1 ± 1.9	10.2 ± 0.5	2.4 ± 0.3	9.8 ± 0.8	6.5 ± 0.6
34.7	68.0 ± 1.8	11.3 ± 0.5	2.2 ± 0.3	11.0 ± 0.8	7.5 ± 0.7

Results

The percentages for each of the product ions are collected in Table 1 as a function of the collision energy. We note that these percentages are calculated with respect to the total number of trajectories that dissociated during the 5-ps integration time, that is, those halted by criterion a; therefore, we do not include here those trajectories counted as reactive on the basis of energetic (criterion c) or statistical (criterion d) grounds (see Table 2). The percentages of products in which hydrogen migration occurred (not shown in Table 1) are 0−2% for CH_3^+ formation, 20−53% for CH_2SH^+, 23−57% for CH_2S^+, and 0−17% for CH_3S^+. To calculate these percentages, we considered only those collision energies in which we had at least 10 reactive events for each fragment. From these results, it is clear that hydrogen migration is significant in the CH_3SH^+ dissociation, especially for the production of CH_2SH^+ and CH_2S^+. Furthermore, the above values are lower bounds because trajectories halted by criteria c and d, which account for 16−36% of the total number of reactive trajectories, have, in general, longer lifetimes so that hydrogen migration is even more likely to take place. If we assume that H migration occurs in these trajectories, then we estimate that at 8.7 eV the upper bound for the percentage of trajectories leading to CH_2SH^+ formation that are experiencing H migration is 70%. This is an interesting process that was neglected in our previous QCT calculations.[11]

The average lifetimes for each of the fragmentation channels are listed in Table 3. We did not include the average lifetime for CH_2S^+ formation in the table because of the small number of trajectories undergoing this process. As can be seen, the

TABLE 2: Percentages of Reactive Trajectories Halted by Criteria a, c, and d

	collision energy (eV)													
criterion[a]	6.5	8.7	10.8	13.0	15.2	15.4	19.5	21.7	23.9	26.0	28.2	30.4	32.5	34.7
a	64	67	74	75	75	78	79	80	82	81	83	83	84	84
c	30	26	20	18	18	15	14	13	13	13	11	11	10	11
d	6	7	6	7	7	7	7	7	5	6	6	6	6	5

[a] See QCT details.

TABLE 3: Average Lifetimes[a] (in fs) for Each of the Fragmentation Channels as a Function of Collision Energy

	collision energy (eV)													
products	6.5	8.7	10.8	13.0	15.2	15.4	19.5	21.7	23.9	26.0	28.2	30.4	32.5	34.7
CH_3^+	1285	945	668	581	521	477	396	384	364	355	328	354	363	310
CH_2SH^+				1594	1461	1687	1411	1247	1418	1131	1137	1266	1215	1159
CH_2^+							228	230	200	163	177	138	132	165
CH_3S^+										384	153	176	218	255

[a] The lifetime was computed as the time interval between the instant of collision, as defined in ref 11, and the time at which the fragments were separated by 6 Å. The lifetimes were computed only when the number of dissociating trajectories was larger than 50.

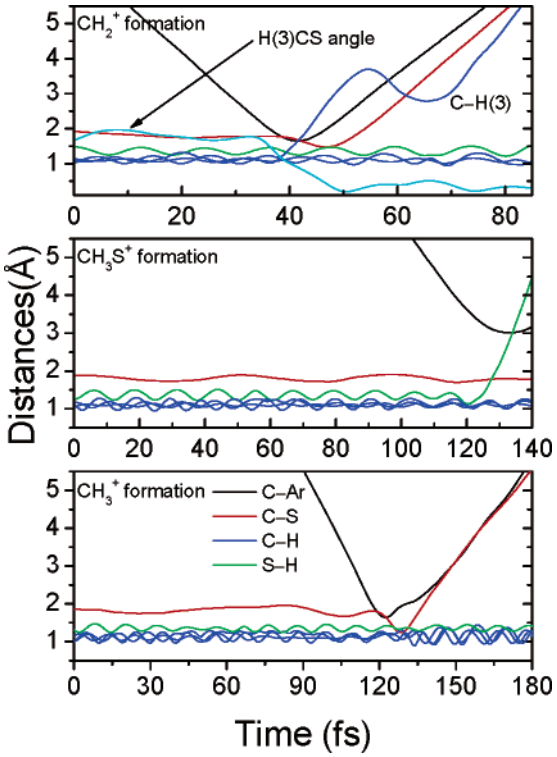

Figure 4. Three typical trajectories showing the shattering mechanism for CH_2^+, CH_3S^+, and CH_3^+ formation at a collision energy of 21.7 eV. The H(3)CS angle is given in radians.

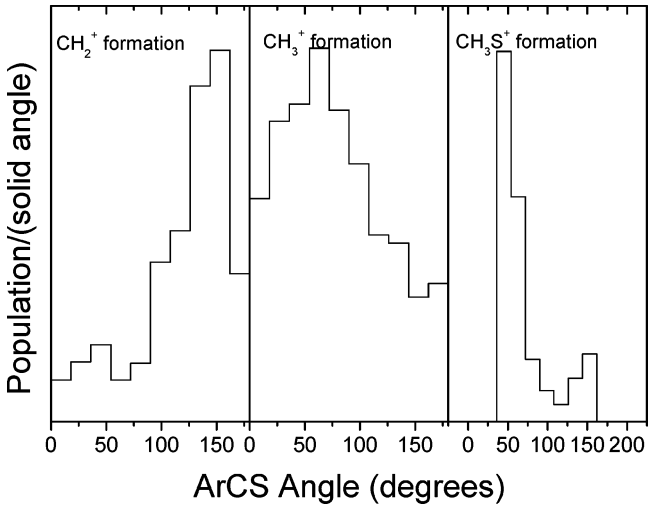

Figure 5. ArCS angle populations per solid angle at the time of collision for the CH_2^+, CH_3S^+, and CH_3^+ formation processes at a collision energy of 21.7 eV.

formation of CH_3^+, CH_2^+, and CH_3S^+ is very fast, with lifetimes of the order of several femtoseconds, whereas the formation of CH_2SH^+ and CH_2S^+ is slower. These results are consistent with the fact that hydrogen migration is significant in the production of the last two cations.

The marked differences in the average lifetimes are an indication of different fragmentation mechanisms. Similar to what we found in our previous QCT study,[11] in the present study the production of CH_3^+, CH_3S^+, and CH_2^+ occurs primarily by a "shattering" mechanism, in which the fragments are formed just after the collision, without time for randomization of the energy within the excited CH_3SH^+ molecule. Specifically, at 21.7 eV the percentage of trajectories that followed this mechanism is more than 80% for CH_2^+, CH_3^+, and CH_3S^+ and less than 30% for CH_2SH^+ and CH_2S^+ (note that these values were evaluated from trajectories halted by criterion a only).

Figure 4 shows three typical shattering trajectories for the CH_2^+, CH_3S^+, and CH_3^+ dissociation channels. The most surprising mechanism is that of CH_2^+ formation in which an H atom migrates from the C to the S atom in about 15 fs and, right after this event, the C−S bond breaks. The process seems to take place in a concerted, nonsynchronous way. These striking events occur preferentially when the Ar atom collides forming an Ar−C−S angle of about 140°, as shown in Figure 5. For the formation of CH_3S^+, as expected, the favorable orientation of Ar at the instant of collision is near the S−H group (i.e., for low Ar−C−S angles). The mechanism for CH_3^+ formation shows an essentially side-on preference (see Figure 5), but its directionality character is not as strong as those presented by CH_2^+ and CH_3S^+ formation.

More features on the dynamics of the title reaction can be extracted from Figure 6 in which we show angle-velocity distributions of the scattered CH_2SH^+ (plots a−c) and CH_3^+ (plots d−f) cations, represented as polar product scattering maps. As can be seen, as the collision energy increases both products are more forward scattered. The effect is more pronounced for CH_2SH^+ because the opacity function for the formation of this cation, shown in Figure 7, is shifted toward higher values of *b* as the collision energy increases, whereas the corresponding function for CH_3^+ does not change significantly with the collision energy. Therefore, as the collision energy increases,

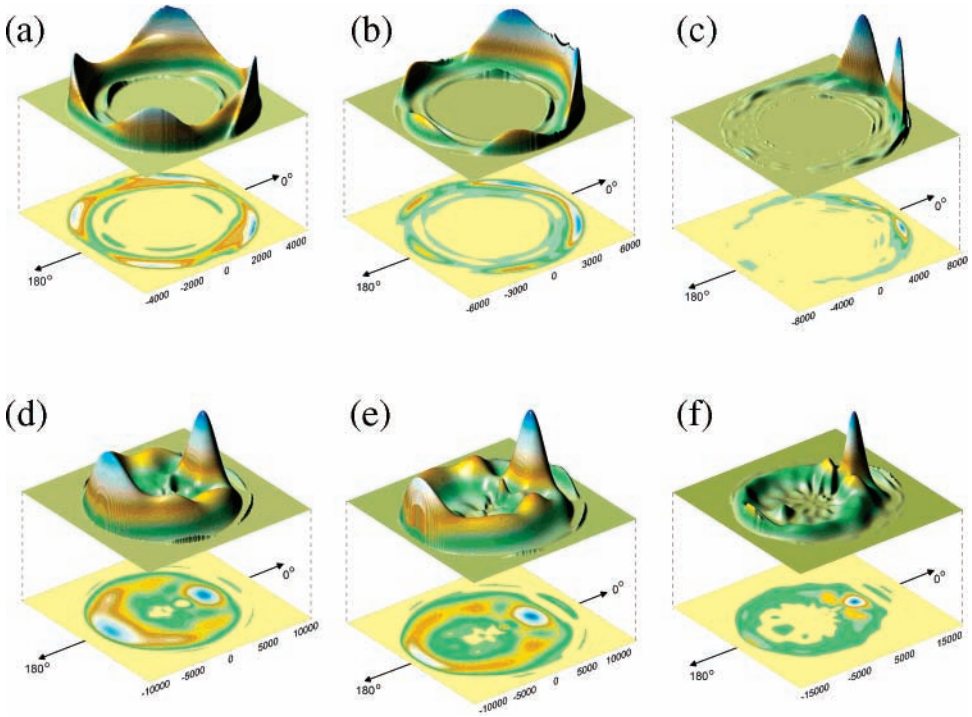

Figure 6. Polar velocity maps for products CH_2SH^+ and CH_3^+ at collision energies of 13.0 eV (plots a and d, respectively), 21.7 eV (plots b and e, respectively), and 34.7 eV (plots c and f), respectively.

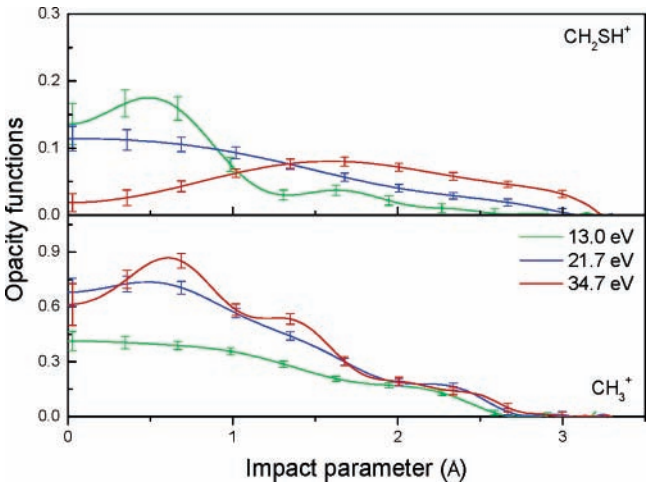

Figure 7. Opacity functions for products CH_2SH^+ and CH_3^+ at different collision energies.

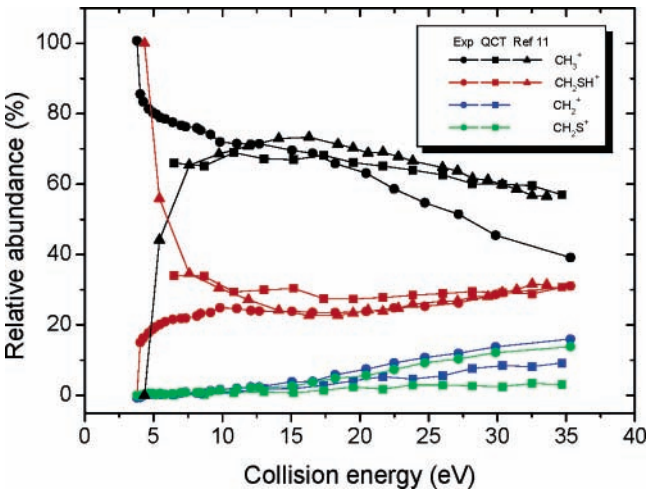

Figure 8. Relative abundances of CH_3^+, CH_2SH^+, CH_2^+, and CH_2S^+ obtained in this study in comparison with the CID results of ref 1 and our previous QCT calculations of ref 11.

the number of grazing collisions leading to CH_2SH^+ formation increases and, as a result, the scattering becomes more forward. It is also clear from Figure 6 that the distributions of speeds of the CH_3^+ cations are broader than those of CH_2SH^+. This result may be expected because for the $CH_3^+ + SH$ dissociation there are more degrees of freedom in which the internal energy of the scattered CH_3SH^+ can be distributed. Furthermore, the internal energy distribution of CH_3SH^+ ions producing $CH_2SH^+ + H$ is narrow because in this case the number of grazing collisions is greater, as explained above.

The experimental and theoretical relative abundances of product ions CH_3^+, CH_2SH^+, CH_2^+, and CH_2S^+ are compared in Figure 8. We also included the previous QCT results, which were normalized to the theoretical populations of CH_3^+ and CH_2SH^+ obtained in the present study. Despite the improvement in the intramolecular potential energy surface with the inclusion of additional reactive channels and the importance of hydrogen migration, the present QCT results predict similar CH_3^+/CH_2SH^+ relative abundances. Particularly, at the energies of our study, CH_3^+ is 2−3 times more abundant than CH_2SH^+. Although the present cross sections for the formation of CH_3^+ at energies higher than ~15 eV are slightly lower than those calculated in the previous QCT study,[11] as shown in Figure 9; in general, both QCT results are very similar to each other and significantly higher than the experimental values. There may be several sources of disagreement, and some of them are discussed as follows. First, presumably the experimental data only takes into account those ions dissociating within the time-of-flight in their triple-quadrupole double-octopole photoionization ion−molecule apparatus. Second, as pointed out elsewhere,[21,22] it is known that the experimental cross sections are possibly somehow too small because some strongly sideways-scattered product ions are not detected. However, these possible sources of discrepancy probably cannot fully account for the large differences between theory and experiment. The major

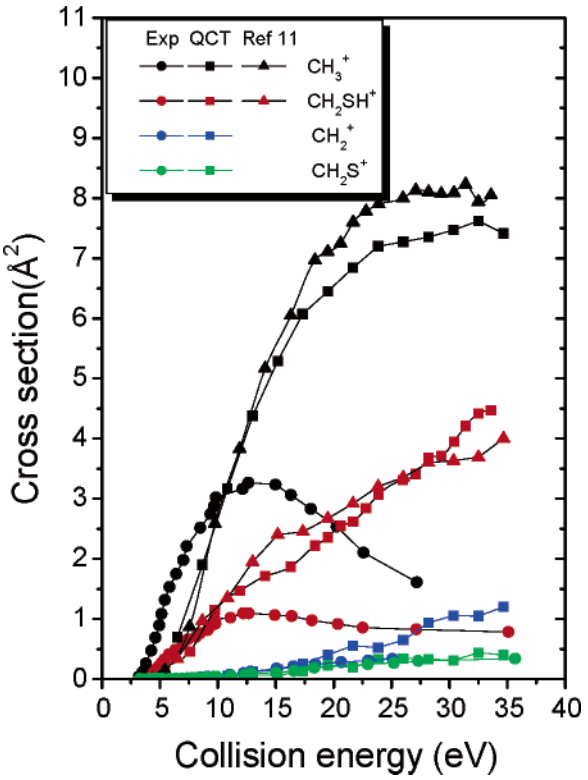

Figure 9. Absolute cross sections for the formations of CH_3^+, CH_2SH^+, CH_2^+, and CH_2S^+ obtained in this study in comparison with the experimental CID results of ref 1 and our previous QCT calculations of ref 11.

source of disagreement seems to be that our model calculations overestimate the transfer of translational to vibrational energy. The comparison between the theoretically predicted and experimental product abundances, however, is reasonably good, particularly for CH_2SH^+; but as the energy becomes increasingly higher (from ca. 15 eV), the experimental percentage of CH_3^+ decreases more rapidly than the theoretical predictions. Concomitantly, the relative abundances of CH_2^+ and CH_2S^+ calculated in the present study increase more slowly with the collision energy than do the experimental ones. The crossing point obtained in the previous QCT calculations (see Figure 7) was discussed in ref 11. Unfortunately, in the present work the calculations at very low collision energies are very costly in CPU time (mainly because a very large number of trajectories are needed for good statistics), which prevented us from investigating the behavior at collision energies down to 6.5 eV. However, from the classical dynamics model, one would expect a crossing point at a collision energy close to the dissociation energy of the $CH_3^+ + SH$ channel. The fact that the first appearance energy observed in the experiment[1,2] corresponds to the $CH_3^+ + SH$ channel is very striking and might be due to insufficient sensitivity of the detector.

Conclusions

The dynamics of the dissociation of CH_3SH^+ induced by collisions with Ar atoms was studied by classical trajectories at collision energies ranging from 6.5 to 34.7 eV. The intramolecular part of the potential energy surface comprises seven reaction channels, and was constructed by interpolating 3000 data points at the MP2/6-311G(d,p) level of theory. The calculations indicate that the rearrangement $CH_3SH^+ \leftrightarrow CH_2SH_2^+$, due to migration of hydrogen atoms, is substantial at the selected collision energies (6.5−34.7 eV). Channels leading to CH_3^+, CH_3S^+, and CH_2^+ cations occur mainly by a shattering mechanism, that is, the products are formed immediately after the collision.

At the collision energies investigated, $CH_3^+ + SH$ is the most reactive channel, as observed experimentally. The results are in line with those obtained in our previous QCT study (on a simpler model PES)[11] and corroborate the previous suggestion of Ng and co-workers[1−3] that the energy transfer mechanism and the dissociation dynamics for the title reaction are highly nonstatistical.

The present QCT calculations yield integral cross sections that are noticeably smaller than the experimental absolute cross sections, which may be due to inaccuracies in the PES employed in the QCT calculations. However, the calculated relative abundances of the product ions are in qualitative agreement with the experimental yields. The absolute cross sections and CH_2SH^+/CH_3^+ ratios obtained with the present PES are very much consistent with those calculated in our previous QCT study using a simpler analytical PES.

The angle-velocity distributions of the scattered CH_2SH^+ and CH_3^+ ions show a preference for forward scattering as the collision energy increases. The speed distributions for the former cation are narrower than those for the latter, presumably because this species contains almost all of the mass of the parent CH_3SH^+ ion.

Acknowledgment. E.M.-N. and J.F.C. thank the Spanish Ministry of Education and Science for their Ramón y Cajal research contracts. Time allocation for part of the calculations was provided generously by "Centro de Supercomputation de Galicia" (CESGA). F.J.A. and J.F.C. acknowledge financial support by the Ministry of Education of Spain Grant BQU2002-04627-C02.

References and Notes

(1) Fenn, T.; Chen, Y.-J.; Stimson, S.; Ng, C.-Y. *J. Phys. Chem. A* **1997**, *101*, 6513.

(2) Chen, Y.-J.; Fenn, P. T.; Stimson, S.; Ng, C.-Y. *J. Chem. Phys.* **1997**, *106*, 8274.

(3) Ng, C.-Y. *J. Phys. Chem. A* **2002**, *106*, 5953.

(4) Amos, D.; Gills, R. G.; Occolowitz, J. L.; Pissani, J. F. *Org. Mass. Spectrom.* **1969**, *2*, 209.

(5) Holmes, J. L.; Lossing, F. P.; Terlouw, J. K.; Burgers, P. C. *Can. J. Chem.* **1983**, *61*, 2305.

(6) Kutina, R. E.; Edwards, A. K.; Berkowitz, J. *J. Chem. Phys.* **1982**, *77*, 5508.

(7) Jonsson, B.-Ö.; Lind, J. *J. Chem. Soc., Faraday Trans. 2* **1974**, *70*, 1399.

(8) Nourbakhsh, S.; Norwood, K.; Yin, H.-M.; Liao, C.-L.; Ng, C. Y. *J. Chem. Phys.* **1991**, *95*, 945.

(9) Martínez-Núñez, E.; Vázquez, S. A. *J. Phys. Chem. A* **1999**, *103*, 9783.

(10) Martínez-Núñez, E.; Peña-Gallego, A.; Rodríguez-Fernández, R.; Vázquez, S. A. *Chem. Phys. Lett.* **2000**, *324*, 88.

(11) Martínez-Núñez, E.; Vázquez, S. A.; Marques, J. M. C. *J. Chem. Phys.* **2004**, *121*, 2571.

(12) Frisch, M. J.; Trucks, G. W.; Schlegel, H. B.; Scuseria, G. E.; Robb, M. A.; Cheeseman, J. R.; Zakrzewski, V. G.; Montgomery, J. A., Jr.; Stratmann, R. E.; Burant, J. C.; Dapprich, S.; Millam, J. M.; Daniels, A. D.; Kudin, K. N.; Strain, M. C.; Farkas, O.; Tomasi, J.; Barone, V.; Cossi, M.; Cammi, R.; Mennucci, B.; Pomelli, C.; Adamo, C.; Clifford, S.; Ochterski, J.; Petersson, G. A.; Ayala, P. Y.; Cui, Q.; Morokuma, K.; Malick, D. K.; Rabuck, A. D.; Raghavachari, K.; Foresman, J. B.; Cioslowski, J.; Ortiz, J. V.; Stefanov, B. B.; Liu, G.; Liashenko, A.; Piskorz, P.; Komaromi, I.; Gomperts, R.; Martin, R. L.; Fox, D. J.; Keith, T.; Al-Laham, M. A.; Peng, C. Y.; Nanayakkara, A.; Gonzalez, C.; Challacombe, M.; Gill, P. M. W.; Johnson, B. G.; Chen, W.; Wong, M. W.; Andres, J. L.; Head-Gordon, M.; Replogle, E. S.; Pople, J. A. *Gaussian 98*, revision A.7; Gaussian, Inc.: Pittsburgh, PA, 1998.

(13) Jordan, M. J. T.; Thompson, K. C.; Collins, M. A. *J. Chem. Phys.* **1995**, *102*, 5647.

(14) Thompson, K. C.; Jordan, M. J. T.; Collins, M. A. *J. Chem. Phys.* **1998**, *108*, 8302.
(15) Bettens, R. P. A.; Collins, M. A. *J. Chem. Phys.* **1999**, *111*, 816.
(16) Martínez-Núñez, E.; Vázquez, S. A. *J. Mol. Struct.: THEOCHEM* **2000**, *505*, 109.
(17) Nyman, G. S.; Nordholm, S.; Schranz, H. W. *J. Chem. Phys.* **1990**, *93*, 6767.
(18) Schranz, H. W.; Nordholm, S.; Nyman, G. *J. Chem. Phys.* **1991**, *94*, 1487.
(19) Bolton, K.; Hase, W. L.; Peslherbe, G. H. *Modern Methods for Multidimensional Dynamics in Chemistry*; World Scientific: Singapore, 1998.
(20) Peslherbe, G. H.; Wang, H.; Hase, W. L. *Adv. Chem. Phys.* **1999**, *105*, 171.
(21) Liu, J.; Van Devener, B.; Anderson, S. L. *J. Chem. Phys.* **2002**, *116*, 5530.
(22) Liu, J.; Song, K.; Hase, W. L.; Anderson, S. L. *J. Chem. Phys.* **2003**, *119*, 3040.